J Mater Sci: Mater Electron
DOI 10.1007/s10854-017-7745-1

Facile synthesis of high-performance $Ni(OH)_2$/expanded graphite electrodes for asymmetric supercapacitors

Jiawei Yuan[1,2] · Shuihua Tang[1,2] · Zhentao Zhu[1,2] · Xiaolong Qin[1,2] · Renjie Qu[1,2] · Yuxiao Deng[1,2] · Lingshan Wu[1,2] · Jie Li[1,2] · Geir Martin Haarberg[3]

Received: 7 June 2017 / Accepted: 17 August 2017

Abstract Cost-effective commercial expanded graphite (EG) was used as a raw material, and a facile in-situ electrodeposition method was adopted to synthesize a layered $Ni(OH)_2$/EG composite electrode in an *N,N*-dimethylformamide-water system. Scanning electron microscopy images show that expanded graphite sheets, $Ni(OH)_2$ nanoparticles and carbon nanotubes construct a layered structure, which not only effectively restrains restacking of EG sheets but also prevents aggregation of nickel hydroxide particles. The electrode delivers a satisfactory initial specific capacitance of 1719.5 F/g at 1 A/g with a total mass loading of 5.0 mg/cm^2. Even at 10 A/g, the capacitance only decreases to 1181.3 F/g, showing a remarkable rate capability. Moreover, an optimized asymmetric supercapacitor (ASC) device was fabricated, in which the $Ni(OH)_2$/EG electrode was used as a positive electrode and commercial activated carbon (AC) was used as a negative electrode. The ASC device can deliver a prominent energy density of 32.3 Wh/kg at power density 504.7 W/kg, and long cycling life with 79% original capacitance after 1000 cycles at 5 A/g, which can be prospective to be applied in practical devices for energy storage and conversion.

✉ Shuihua Tang
spraytang@hotmail.com

[1] State Key Lab of Oil and Gas Reservoir Geology & Exploitation, Southwest Petroleum University, Chengdu 610500, People's Republic of China

[2] School of Materials Science and Engineering, Southwest Petroleum University, Chengdu 610500, People's Republic of China

[3] Department of Materials Science and Engineering, Norwegian University of Science and Technology, 7491 Trondheim, Norway

1 Introduction

Recently, severe environmental issues and energy depletion have pushed the development of green and sustainable energy storage and conversion devices [1–3]. As a promising candidate, supercapacitors (SCs) have received significant attention owing to their excellent cycling lifespan, high power density, fast charge/discharge rate, environmental benignity and safe usage [4–7]. However, low energy density and high costs restrict their wide applications in energy storage. Developing novel electrode materials which have a high specific capacitance and low price to increase device capacitance or assembling asymmetric supercapacitor (ASC) to broaden the cell voltage is an effective strategy to address this problem on the basis of the equation of energy density (*E*) $E = 1/2\ CV^2$ [8].

Owing to their well-defined redox activity, desirable theoretical capacitance and environmental friendliness, nickel hydroxide has been extensively investigated recently [9–11]. Unfortunately, the poor electronic conductivity (10^{-17} S/cm) of nickel hydroxides hinders electron transfer and reduces the efficiency of redox reactions, leading to low power densities and rate capabilities [12]. Thus, a facile approach to enhance the capacitive performances of nickel hydroxide is to introduce high conductive carbon materials. Activated carbon (AC) [13–15], carbon nanotubes (CNTs) [16–19], graphene (GR) [20–25], expanded graphite (EG) [26] and Vulcan XC-72 [27] have been widely investigated. Besides, tremendous works have been done to fabricate aqueous electrolyte-based ASC by using nickel hydroxide-carbon composites as the positive electrode and commercial AC as the negative electrode material (denoted as AC//$Ni(OH)_2$/C). Examples of these are AC//$Ni(OH)_2$/GR [28], AC//$Ni(OH)_2$/CNT/AC [29], AC//$Ni(OH)_2$/$Co(OH)_2$/GR

Published online: 20 August 2017

[30], AC//$Ni(OH)_2$/CNT [17]. These ASCs exhibit a high voltage window and energy density.

EG has been investigated owing to its unique properties in terms of excellent electrical conductivity, good chemical stability, low price, relatively wider interlayer spacing and the larger specific surface area as compared to graphite [31]. Guo et al. [32] prepared AC/EG composite by a novel supersonic wave shocking method, the largest specific capacitance (*Cs*) can reach to 305 F/g at 1 mA charging current. Besides, Xu et al. [26] synthesized NiO/EG composite via a chemical precipitation method, the *Cs* is 510 F/g at 0.1 A/g. However, poor capacitive performance of electrode material prepared from EG is the most pressing problem which needs to be solved.

In this work, low-cost EG will be used as a carbon material, carbon nanotubes (CNTs) will be added as a conductive agent, then the EG and CNTs dispersion will be dropped onto a nickel mesh substrate to fabricate an EG electrode. Later the EG electrode will be immersed in a $Ni(NO_3)_2$ solution and in-situ electrodeposited to obtain a layered nickel hydroxide/EG composite electrode. Moreover, an optimized AC//$Ni(OH)_2$/EG device will be assembled and its electrochemical performances will be investigated.

2 Experimental

2.1 Preparation of materials

Firstly, nickel foam (10 mm × 10 mm, Changsha Liyuan New Material Co., Ltd) was ultrasonically cleaned with acetone, deionized water and ethanol for 30 min, then vacuum dried at 70 °C. Secondly, EG/CNTs slurry was obtained by mixing EG, CNTs (Chengdu Organic chemicals Co., Ltd, as a conductive agent) and Nafion® solution (Du Pont Company, as a binder) with a mass ratio of 85:10:5. The slurry was ultrasonically stirred until a homogeneous dispersion was obtained. Then the slurry was dropped uniformly onto the Ni foam substrate, controlling a mass loading of EG, CNTs and Nafion solution was 2.0 mg/cm^2, and dried at 70 °C overnight. Finally, the electrodeposition of nickel hydroxide was conducted in a conventional three-electrode cell, which consisted of a nickel foam plate (20 mm × 20 mm) counter electrode, a saturated calomel electrode reference (SCE) electrode and as-prepared EG working electrode. An Autolab potentiostat 302N (Metrohm Holland) was used to perform electrochemical measurements. The potential was set at −1.1 V versus SCE electrode while the deposition time was fixed as 720 s, and the electrolyte solution was 0.1 M $Ni(NO_3)_2{\cdot}6H_2O$ in a 1:10 (v/v) H_2O/DMF mixed solvent. The electrodeposition was conducted at room temperature. After the electrodeposition, the obtained electrode was rinsed with deionized water and dried at 70 °C overnight in a vacuum oven. Finally, the mass loading of deposition production was 3.0 mg/cm^2.

The preparation of $Ni(OH)_2$ nanoparticles includes an electrochemical and a chemical process. The NO_3^- anions from the electrolyte solution can be electrochemically reduced on the cathode to produce OH^- anions. These formed OH^- groups react with Ni^{2+} cations to form $Ni(OH)_2$ precipitation, and the entire process can be described by the following steps [33]:

$$NO_3^- + 7\,H_2O + 8\,e^- \rightarrow NH_4^+ + 10\,OH^-$$

$$2\,OH^- + Ni^{2+} \rightarrow Ni(OH)_2$$

2.2 Characterization

The prepared materials was characterized using Philips X' pert pro MPD X-ray diffraction (XRD, Cu, k = 0.15406 nm). The morphology and microstructures of EG and prepared electrode were observed using a Zeiss scanning electron microscope (SEM, EVO MA15) and a Hitachi Field emission scanning electron microscope (FESEM, JSM-7500F/X-MAX50). The typical morphologies of prepared material were obtained from Zeiss Transmission electron microscope (TEM, LiBRA 200FE). Infrared spectroscopy was carried out using a Fourier transform infrared spectrometer (FT-IR, Nicolet 6700).

2.3 Assembly of asymmetric supercapacitor (ASC) device

An AC//$Ni(OH)_2$/EG device, with a negative electrode of commercial activated carbon (AC) and a positive electrode of the $Ni(OH)_2$/EG, was fabricated in a two-electrode configuration. The nonwoven fabrics (NKK company, Japan) were used as the diaphragm. The AC electrode was obtained by mixing 80 wt% of the commercial AC, 10 wt% CNTs and 5 wt% polytetrafluoroethylene (PTFE) in ethanol and brushed onto a Ni foam substrate (Φ = 14 mm) before being dried at 80 °C. Then the electrode materials and diaphragm were soaked in 6 M KOH electrolyte overnight before assembly.

2.4 Electrochemical studies

Electrochemical studies of the $Ni(OH)_2$/EG and AC electrode were carried out on an Autolab potentiostat 302N in a traditional three-electrode system, with the obtained electrode as working electrode, Pt coil as counter electrode and Hg/HgO as reference electrode. 6 M KOH solution was used as electrolyte. The *Cs* can be estimated by cyclic voltammetry (CV) or galvanostatic charge–discharge (GCD) curves based on Eqs. (1) and (2), respectively:

$$Cs = \int IdV / 2m\vartheta\Delta V \tag{1}$$

$$Cs = I \times \Delta t / m \times \Delta V \tag{2}$$

where Cs (F/g), I (A), m (g), Δt (s) represent the specific capacitance, response current, mass of the electrode materials and discharge time, respectively. ϑ (mV/s) indicates the scan rate and ΔV (V) represents potential window.

The as-assembled ASC device was measured using a two-electrode mode. Electrochemical impedance spectroscopy (EIS) was carried out by applying 5 mV perturbation amplitude versus the open circuit, the frequency was chosen to vary from 100 kHz to 0.01 Hz. The energy density (E) was estimated based on Eq. (3) and power density (P) was obtained by the formula (4) respectively:

$$E = {}^{1}/_{2}Cs \times V^{2} \tag{3}$$

$$P = {}^{E}/_{t} \tag{4}$$

where V (V), Cs (F/g), t (s) represent the voltage window, specific capacitance of total cell and discharge time, respectively.

3 Results and discussion

XRD pattern of $Ni(OH)_2$/EG composite by peeling off the $Ni(OH)_2$/EG electrode is presented in Fig. 1a. Except for three diffraction peaks associated with the nickel foam substrate and one diffraction peak for graphite, no characteristic peaks can be observed from the pattern. It may be suggested that the prepared nickel hydroxide particles are amorphous. Besides, a broad and diffused halo ring associated with nickel hydroxide can be found from selected-area electron-diffraction (SAED) pattern (Fig. 4d inset). The results further demonstrate that nickel hydroxide deposits are an amorphous morphology. Also, the energy dispersive X-ray spectroscope (EDS) spectra (Fig. 1b) show that O, C, and Ni elements are present in the composites.

The FT-IR spectrum of the $Ni(OH)_2$/EG composite is shown in Fig. 2. The characteristic band at 3410 and 3170 cm^{-1} can be assigned to inter-lamellar water and hydroxyl groups, respectively [34]. The broad bands around 3140 and 1623 cm^{-1} are assigned to the N–H stretching vibration and δ-H_2O vibration of the water molecule. The band at 1400 cm^{-1} is the characteristic band of interlayer nitrate anion [35]. The band at 1160 cm^{-1} is attributed to the ν-N–H vibration. Its existence could be due to the DMF in solution. It is worth to note that two bands at low wavenumbers can be observed, corresponding to the Ni-O-H bending vibration at 616 cm^{-1} and Ni–O stretching vibration at 450 cm^{-1}, respectively [36]. These results show that the nickel hydroxide is present in the prepared composite.

The morphologies and structures of EG and $Ni(OH)_2$/EG composite are observed by SEM and TEM. It can

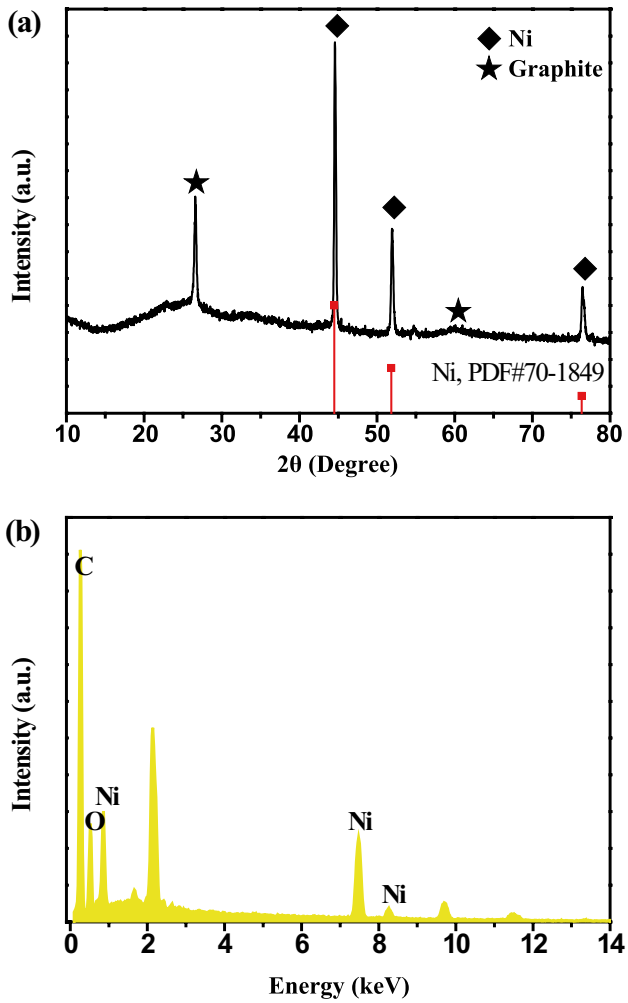

Fig. 1 **a** XRD patterns and **b** EDS spectra of $Ni(OH)_2$/EG composite

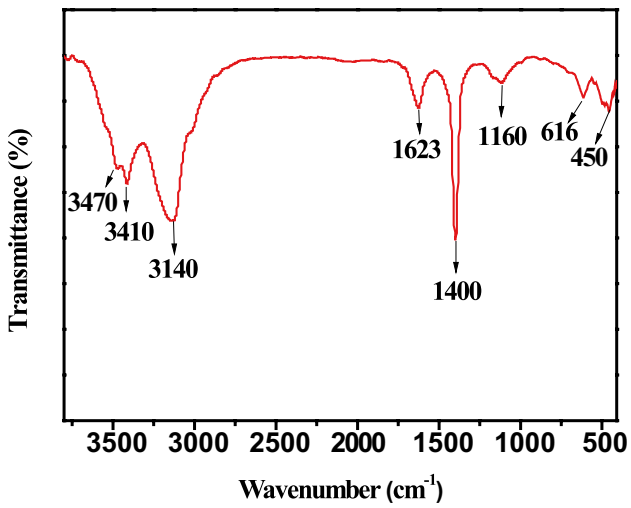

Fig. 2 FT-TR spectra of $Ni(OH)_2$/EG composite

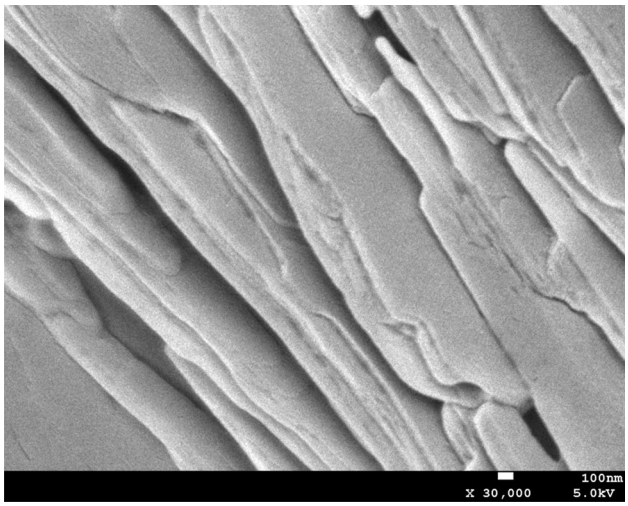

Fig. 3 FESEM image of expanded graphite

be seen from SEM image (Fig. 3) that EG sheets have a layered structure and wide interlayer spacing. The nickel hydroxide nanoparticles can be easily intercalated into the graphite layer by electrochemical deposition. Figure 4a, b show SEM images of $Ni(OH)_2$/EG. The composite exhibits a layered structure, nickel hydroxide particles intercalated into the graphite layer and deposited on the surface of graphite sheets. The embedded nickel hydroxide nanoparticles expand interlayer spacing and create some pore structures, which is beneficial to the infiltration of the electrolyte. The TEM image (Fig. 4c) displays that the EG sheets in the $Ni(OH)_2$/EG are thin and possess some wrinkles, acting as opposite materials to support the nickel hydroxide particles. High-magnification TEM image (Fig. 4d) reveals that most of the nickel hydroxide nanoparticles have an average diameter of 35 nm and homogeneously anchored on EG interlayer. In summary,

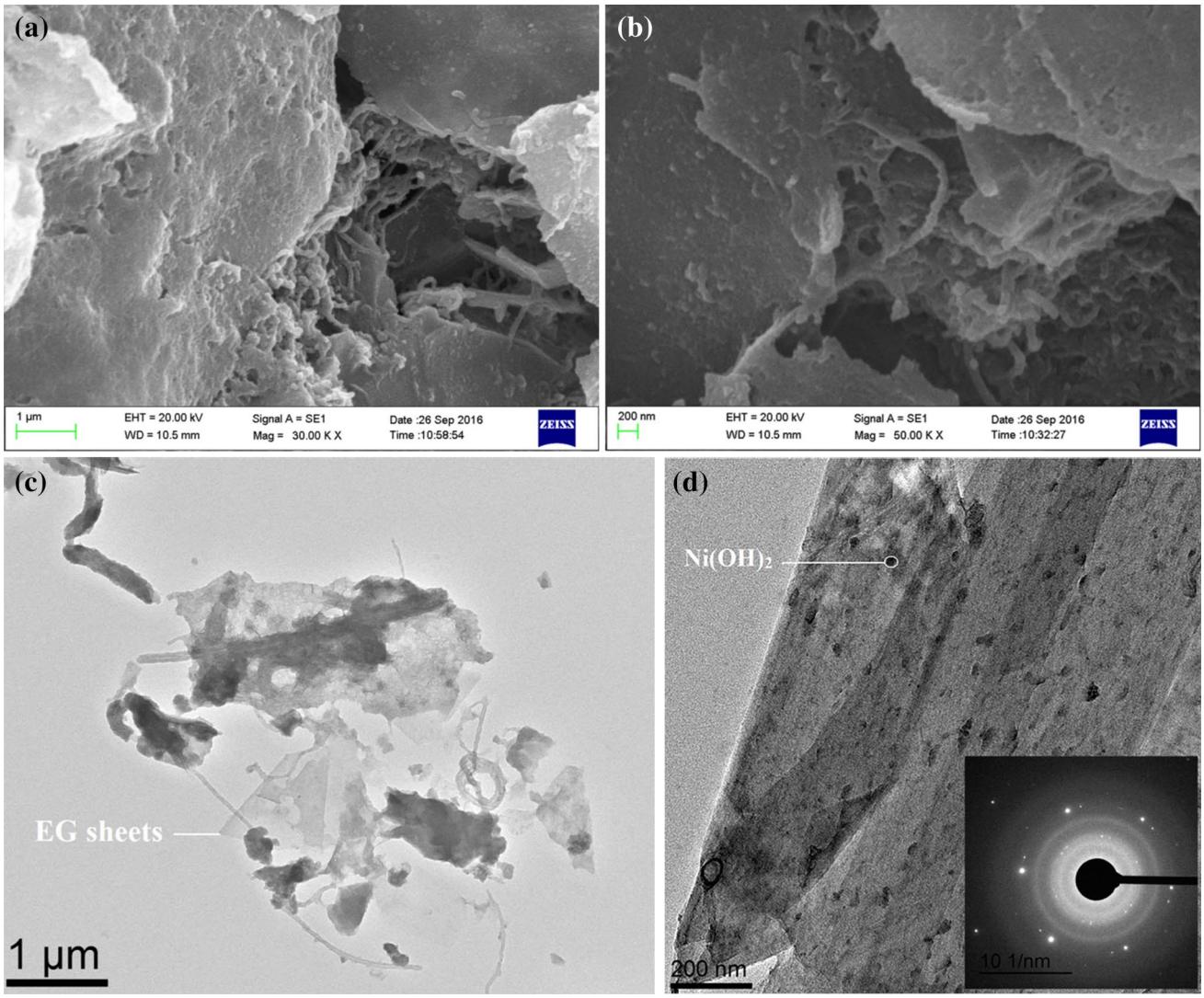

Fig. 4 SEM (**a, b**) and TEM (**c, d**) images of $Ni(OH)_2$/EG composite. Inset image shows selected-area electron diffraction pattern

the XRD, SAED, EDS, FT-IR, SEM and TEM measurements indicate that deposits are amorphous nickel hydroxide nanoparticles. However, the particles exhibit a relatively large particle size, resulting in poor rate performance and cycle life. Further research will be done to obtain smaller nickel hydroxide nanoparticles.

3.1 Electrochemical performances of electrode materials

In order to certify high electrochemical performances of the $Ni(OH)_2$/EG electrode, the capacitances are investigated using CV and GCD tests. Figure 5a displays CV curves of the electrode with various scanning rates (2–20 mV/s), where the potential window is fixed from 0.1 to 0.55 V. It can be observed that all CV curves show a couple of clear redox peaks, which derives from the following Faradic reaction:

$$Ni(OH)_2 + OH^- \leftrightarrow NiOOH + H_2O + e^-$$

Demonstrating that the charge storage is mainly ascribed to the pseudocapacitance resulted from the Faradaic reaction. As noted, the anodic peak shows a remarkable diffusion tail at 20 mV/s. The result indicates a relatively slow charge-transfer process [23]. Additionally, the $Ni(OH)_2$/EG electrode was further investigated at varied current densities ranging from 1 to 10 A/g. As shown in Fig. 5b, the electrode displays a well-defined discharge potential plateau, suggesting an ideal reversibility. .Furthermore, the plots of the *Cs* versus current density (Fig. 5c) were collected for the purpose of revealing the high rate performance of electrode. The *Cs* values were calculated to be 1719.5 F/g at the small current density of 1 A/g based on Eq. (2), while the capacitance still retains 68.7% (1181.3 F/g) at 10 A/g. The remarkable capacitance characteristic mainly derives from the synergistic effect between carbon material and transition metal hydroxides. Additionally, as-prepared $Ni(OH)_2$/EG electrode offers a particular layered structure., which greatly facilitates the rapid diffusion of ions to access the $Ni(OH)_2$ nanoparticles. Moreover, the $Ni(OH)_2$ nanoparticles homogeneously anchored on the interfacial interactions between the EG sheets and CNTs via in-situ electrodeposition, thus providing efficient transport of electrons across the interfaces for fast Faradaic redox reactions to enhance capacitive performances [37].

The CV curves of AC electrode are shown in Fig. 6a, which present a nearly rectangular shape and well maintained even at 20 mV/s. The results indicate that the AC electrode has a typical double-layer capacitor behavior and fast electrolyte diffusion. The GCD curves with different current densities can be observed in Fig. 6b, showing a typical linear relationship between potential and time. The

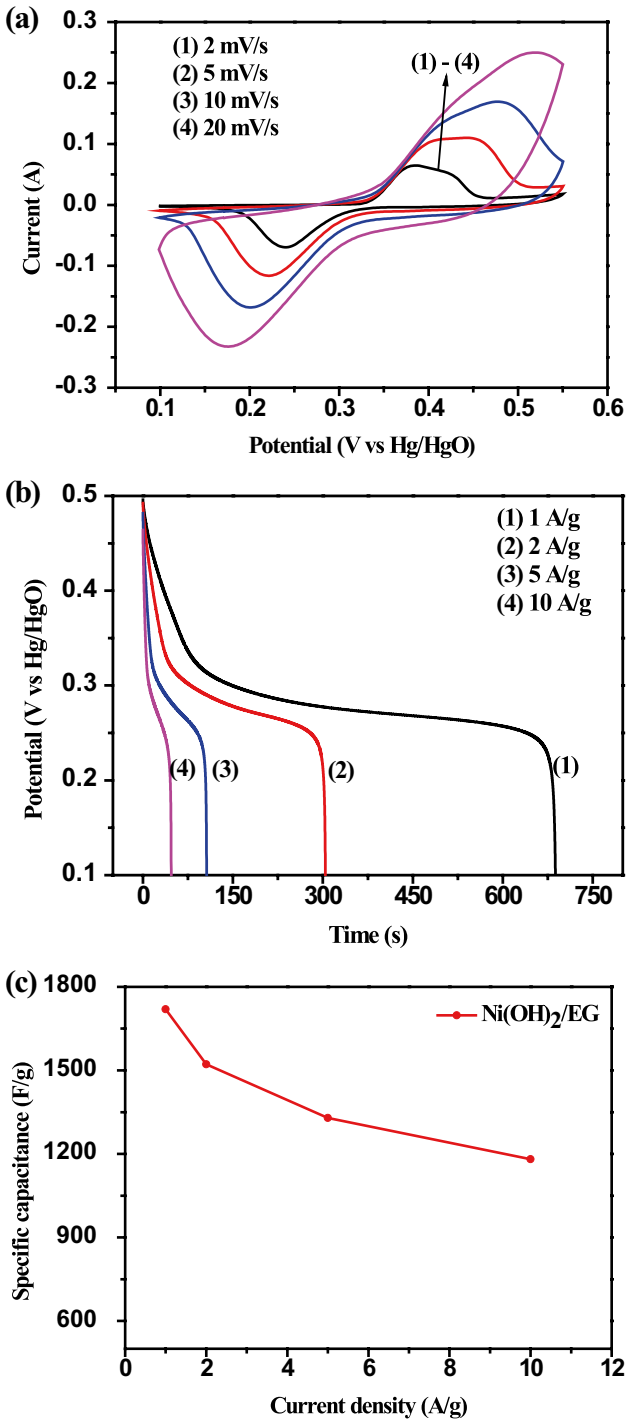

Fig. 5 **a** CV *curves* of $Ni(OH)_2$/EG composite electrode at various scan rates. **b** galvanostatic discharge curves at different current densities and **c** corresponding specific capacitance of $Ni(OH)_2$/EG composite electrode as a function of current densities

calculated *Cs* values of the electrode were 192.5, 173.7, 159.6, 152.2 F/g at 1, 2, 5, 10 A/g based on their discharge time, respectively.

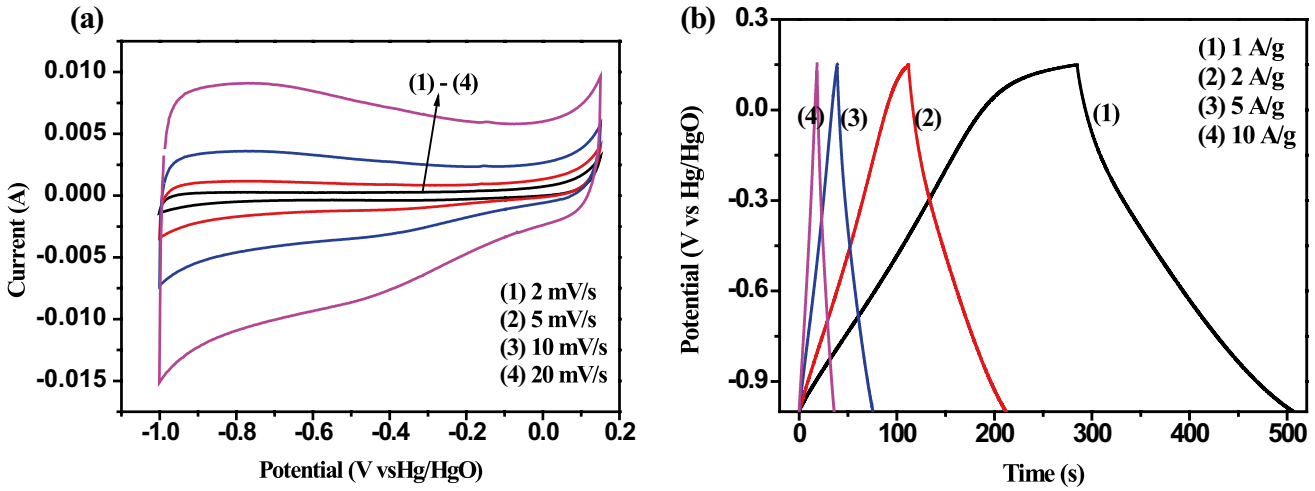

Fig. 6 **a** CV *curves* at various scan rates and **b** GCD *curves* at different current densities of AC electrode

3.2 Electrochemical performances of ASC device

The assembled ASC device can obtain a stable electrochemical voltage of 1.6 V according to CV curves with 2 mV/s scan rate (Fig. 7a). The mass ratio of two electrodes was decided according to the following formula:

$$m_+/m_- = Cs_- \times \Delta V_-/Cs_+ \times \Delta V_+ \quad (5)$$

where m (g), Cs (F/g), ΔV (V) represent the mass of electrode materials, specific capacitance and potential change during charge and discharge process, respectively. From Fig. 7b, the Cs of both negative and positive electrodes was obtained by discharge curves. The mass loading of negative electrodes was 15.0 mg/cm^2 according to the mass loading of positive electrode.

Figure 8a represents the schematic illustration of the assembled ASC, where two electrode materials and diaphragm are stacked into a sandwich-like structure. The CV curves of assembled ACS with various scan rates (5–60 mV/s) can be obtain from Fig. 8b, indicating a collective contribution of double-layer capacitor behavior and pseudocapacitance. Besides, the CV profiles were nearly rectangular and symmetric even when the scan rates reached up to 60 mV/s, indicating a high rate capacity of the as-constructed ASC [38]. As can be seen from Fig. 8c, the GCD profiles of ASC with different current densities show asymmetric triangle patterns, revealing high coulombic efficiency

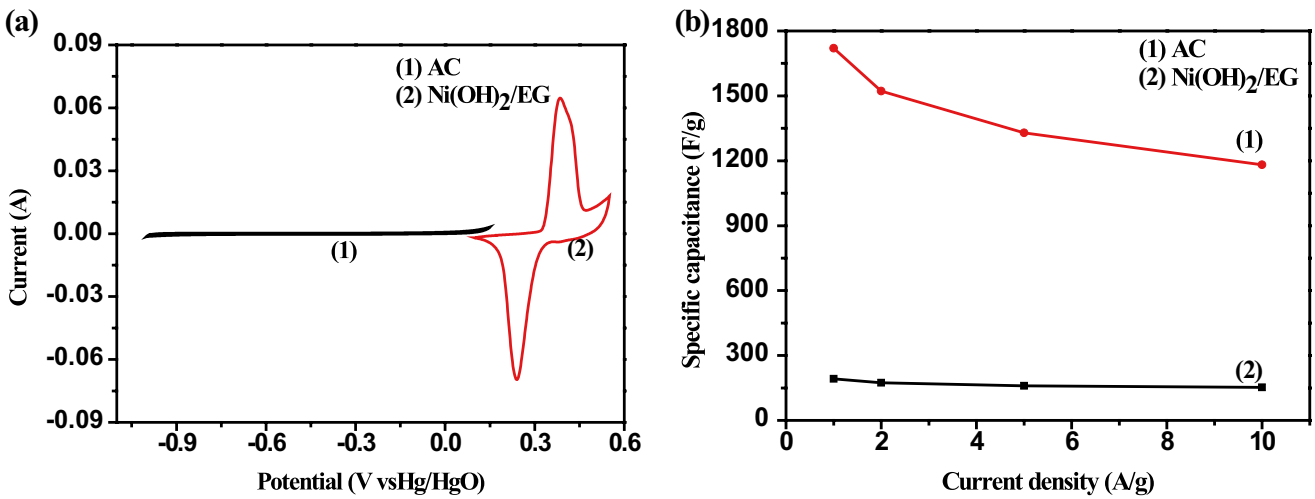

Fig. 7 **a** CV *curves* of AC and Ni(OH)$_2$/EG composite electrode at scan rate of 2 mV/s. **b** Specific capacitances of AC and Ni(OH)$_2$/EG composite electrode at various current densities

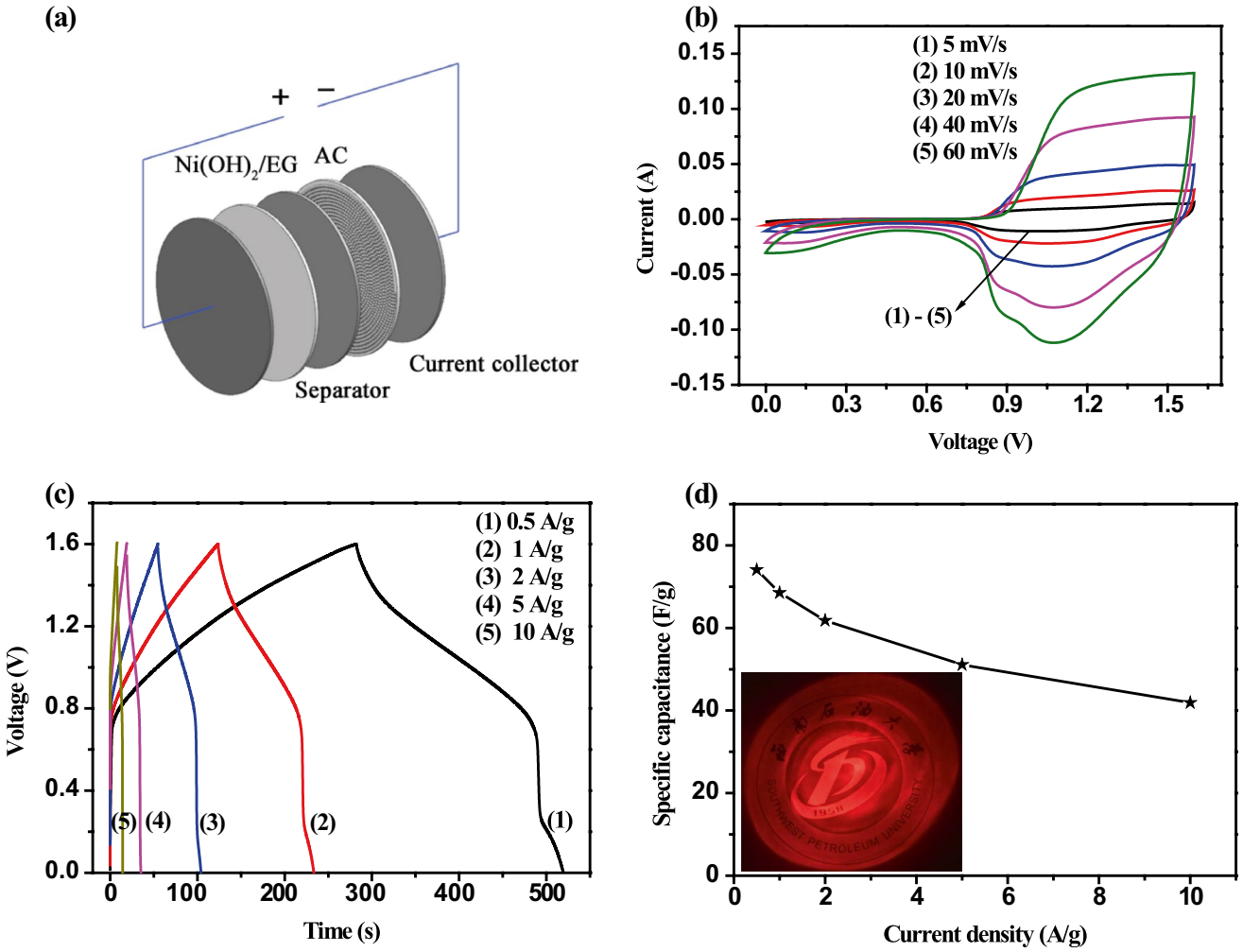

Fig. 8 **a** Schematic of the asymmetric supercapacitor (ASC) device composed of the $Ni(OH)_2$/EG composite and AC electrodes. **b** CV *curves* of the ASC device at different scan rates. **c** GCD *curves* at different current densities of the ASC device. **d** Specific capacitances of the ASC device at various current densities. *Inset* image shows LED lamp

and efficient capacitive behavior. The *Cs* based on discharge curves was calculated according to Eq. (2). As shown in Fig. 8d, the ACS can deliver a *Cs* of 64.6, 57.7, 50.5, 41.1, and 32.5 F/g at 0.5, 1, 2, 5, 10 A/g based on the toll mass of two electrodes, respectively. The high rate performance with 60% capacitance retention was obtained with increasing current density (0.5–10 A/g). It is worth noting that an outstanding energy density (32.3 Wh/kg) can be obtained when the power density reaches 504.7 W/kg based on the Eqs. (3) and (4). In addition, the assembled ACS can light up a red LED lamp (Fig. 8d inset).

The cycle stability of ASC was also evaluated by GCD test (5 A/g) for 1000 cycles. Figure 9a shows that 79% of its initial capacitance is maintained. The results present an excellent stability of assembled ASC. In addition, EIS analysis is performed in order to evaluate electrical resistance. Figure 9b shows Nyquist plots of assembled ASC, which consisted of a semi-circle arcs and a straight line. At the high frequencies, the X-intercept represents the contact/electrolyte resistance (R_s), which is related to the contact resistance and ionic resistance. The R_s values are approximately 0.16 and 0.18 Ω before and after cycling, respectively, demonstrating increasing ohm resistance after 1000 cycles. Besides, the diameter of the semi-circle significantly increased, indicating a higher charge-transfer resistance (R_{ct}) because of collapsing of part of electro-active materials during the harsh redox reaction, which also affects the cycle stability of the ACS [39, 40]. In addition, the slope of the straight line does not change too much after cycling, revealing an ideal capacitor behavior. All results show that the ASC device can demonstrate superior electrochemical performances.

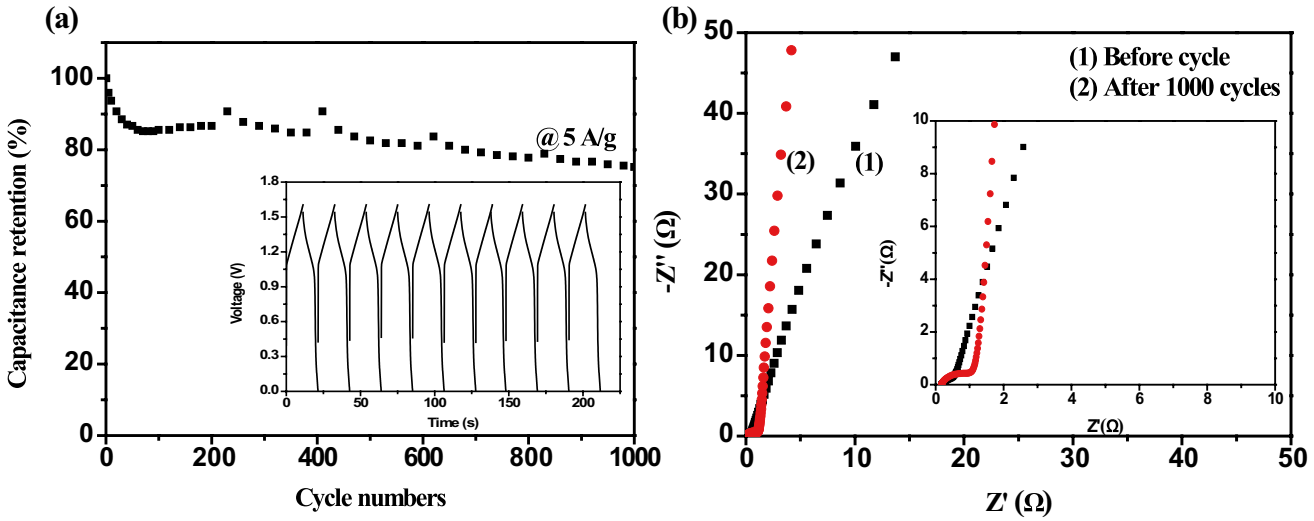

Fig. 9 **a** Cycle performance of the ASC device at current density of 5 A/g. *Inset* image shows the galvanostatic charge–discharge cyclic *curves* of the last 10 cycles. **b** Nyquist plots of EIS before and after 1000 cycles. The *inset* shows the impedance at high frequency region

4 Conclusions

Low cost EG can be used as an effective carbon support. A facile in-situ electrodeposition method was adopted to synthesize a layered $Ni(OH)_2$/EG composite electrode, demonstrating a satisfactory initial *Cs* of 1719.5 F/g at 1 A/g, and remarkable rate capability (1181.3 F/g at 10 A/g). The high capacitive performances primarily derive from the synergistic effect of the layered $Ni(OH)_2$/EG composite. Furthermore, the assembled AC//$Ni(OH)_2$/EG device can deliver a prominent energy density of 32.3 Wh/kg at power density 504.7 W/kg, and long cycling lifespan with 79% original capacitance after 1000 cycles at 5 A/g. These results indicate that the facile synthesized high-performance $Ni(OH)_2$/expanded graphite electrodes could be applied for supercapacitors.

Acknowledgements The support received from the Open Project from State Key Lab of Catalysis (N-14-1), International Technology Collaboration of Chengdu Science and Technology Bureau, Scientific Research Foundation for Returned Scholars, Ministry of Education of China, Innovative Research Team of Southwest Petroleum University (2012XJZT002).

References

1. C.-H. Lai, M.-Y. Lu, L.-J. Chen, J. Mater. Chem. **22**, 19–30 (2012)
2. N.S. Lewis, Science **315**, 798–801 (2007)
3. Y.-G. Guo, J.-S. Hu, L.-J. Wan, Adv. Mater. **20**, 2878–2887 (2008)
4. P. Simon, Y. Gogotsi, Nat. Mater. **7**, 845–854 (2008)
5. M. Winter, R.J. Brodd, Chem. Rev. **104**, 4245–4270 (2004)
6. G. Wang, L. Zhang, J. Zhang, Chem. Soc. Rev. **41**, 797–828 (2012)
7. Y. Wang, Y. Song, Y. Xia, Chem. Soc. Rev. **45**, 5925–5950 (2016)
8. D.P. Dubal, O. Ayyad, V. Ruiz, P. Gomez-Romero, Chem. Soc. Rev. **44**, 1777–1790 (2015)
9. T. Ramesh, R. Jayashree, P.V. Kamath, S. Rodrigues, A. Shukla, J. Power Sources **104**, 295–298 (2002)
10. J. Yan, Z. Fan, W. Sun, G. Ning, T. Wei, Q. Zhang, R. Zhang, L. Zhi, F. Wei, Adv. Funct. Mater. **22**, 2632–2641 (2012)
11. J. Ji, L.L. Zhang, H. Ji, Y. Li, X. Zhao, X. Bai, X. Fan, F. Zhang, R.S. Ruoff, ACS Nano **7**, 6237–6243 (2013)
12. X. Ma, Y. Li, Z. Wen, F. Gao, C. Liang, R. Che, ACS Appl. Mater. Interfaces **7**, 974–979 (2015)
13. J.H. Park, O.O. Park, K.H. Shin, C.S. Jin, J.H. Kim, Electrochem. Solid State Lett. **5**, H7-H10 (2002)
14. Q. Huang, X. Wang, J. Li, C. Dai, S. Gamboa, P. Sebastian, J. Power Sources **164**, 425–429 (2007)
15. M.-H. Kim, J.-W. Lee, S.-M. Park, K.C. Roh, J. Ceram. Process Res. **13**, 265–269 (2012)
16. V.V. Obreja, Phys. E, **40** (2008) 2596–2605
17. Z. Tang, C.h.. Tang, H. Gong, Adv. Funct. Mater. **22**, 1272–1278 (2012)
18. L.L. Zhang, Z. Xiong, X. Zhao, J. Power Sources **222**, 326–332 (2013)
19. R.R. Salunkhe, J. Lin, V. Malgras, S.X. Dou, J.H. Kim, Y. Yamauchi, Nano Energy **11**, 211–218 (2015)
20. H. Wang, Y. Liang, T. Mirfakhrai, Z. Chen, H.S. Casalongue, H. Dai, Nano Res. **4**, 729–736 (2011)
21. Y. Liu, R. Wang, X. Yan, Sci. Rep. **5**, 11095–11106 (2015)
22. L. Mao, C. Guan, X. Huang, Q. Ke, Y. Zhang, J. Wang, Electrochim. Acta **196**, 653–660 (2016)
23. L. Wang, X. Li, T. Guo, X. Yan, B.K. Tay, Int. J. Hydrogen Energy **39**, 7876–7884 (2014)
24. H. Wang, H.S. Casalongue, Y. Liang, H. Dai, J. Am. Chem. Soc. **132**, 7472–7477 (2010)
25. J. Kim, Y. Kim, S.-J. Park, Y. Jung, S. Kim, J. Ind. Eng. Chem. **36**, 139–146 (2016)
26. J. Xu, X. Gu, J. Cao, W. Wang, Z. Chen, J. Solid State Electrochem. **16**, 2667–2674 (2012)
27. L. Sui, S. Tang, Z. Dai, Z. Zhu, H. Huangfu, X. Qin, Y. Deng, G.M. Haarberg, New J. Chem. **39**, 9363–9371 (2015)
28. X. Wang, J. Liu, Y. Wang, C. Zhao, W. Zheng, Mater. Res. Bull. **52**, 89–95 (2014)

29. L. Sui, S. Tang, Y. Chen, Z. Dai, H. Huangfu, Z. Zhu, X. Qin, Y. Deng, G.M. Haarberg, Electrochim. Acta **182**, 1159–1165 (2015)
30. Y. Bai, W. Wang, R. Wang, J. Sun, L. Gao, J. Mater. Chem. A **3**, 12530–12538 (2015)
31. B.H. Ka, S.M. Oh, J. Electrochem. Soc **155**, A685 (2008)
32. C. Guo, C. Wang, Compos. Sci. Technol. **67**, 1747–1750 (2007)
33. G. Helen, Annal Therese, P. Vishnu Kamath, Chem. Mater. **12**, 1195–1204 (2000)
34. M. Taibi, S. Ammar, N. Jouini, F. Fiévet, P. Molinié, M. Drillon, J. Mater. Chem. **12**, 3238–3244 (2002)
35. Y. Ren, L. Gao, J. Am. Ceram. Soc. **93**, 3560–3564 (2010)
36. Y. Li, J. Yao, Y. Zhu, Z. Zou, H. Wang, J. Power Sources **203**, 177–183 (2012)
37. L. Zhang, Q. Ding, Y. Huang, H. Gu, Y.E. Miao, T. Liu, ACS Appl. Mater. Interfaces **7**, 22669–22677 (2015)
38. H. Ma, J. He, D.B. Xiong, J. Wu, Q. Li, V. Dravid, Y. Zhao, ACS Appl. Mater. Interfaces **8**, 1992–2000 (2016)
39. Y. Xu, L. Wang, P. Cao, C. Cai, Y. Fu, X. Ma, J. Power Sources **306**, 742–752 (2016)
40. Y. Zhao, L. Hu, S. Zhao, L. Wu, Adv. Funct. Mater. **26**, 4085–4093 (2016)